SANDIA REPORT

SAND2017-11595
Unlimited Release
Printed October, 2017

Local Varability of the Peierls Barrier of Screw Dislocations in Ta-10W

Stephen M. Foiles

Prepared by
Sandia National Laboratories
Albuquerque, New Mexico 87185 and Livermore, California 94550

Sandia National Laboratories is a multimission laboratory managed and operated by National Technology and Engineering Solutions of Sandia, LLC., a wholly owned subsidiary of Honeywell International, Inc., for the U.S. Department of Energy's National Nuclear Security Administration under contract DE-NA0003525.

Sandia National Laboratories

Issued by Sandia National Laboratories, operated for the United States Department of Energy by National Technology and Engineering Solutions of Sandia, LLC.

Available to DOE and DOE contractors from
U.S. Department of Energy
Office of Scientific and Technical Information
P.O. Box 62
Oak Ridge, TN 37831

Telephone: (865) 576-8401
Facsimile: (865) 576-5728
E-Mail: reports@adonis.osti.gov
Online ordering: http://www.osti.gov/bridge

Available to the public from
U.S. Department of Commerce
National Technical Information Service
5285 Port Royal Rd
Springfield, VA 22161

Telephone: (800) 553-6847
Facsimile: (703) 605-6900
E-Mail: orders@ntis.fedworld.gov
Online ordering: http://www.ntis.gov/help/ordermethods.asp?loc=7-4-0#online

SAND2017-11595
Unlimited Release
Printed October, 2017

Local Varability of the Peierls Barrier of Screw Dislocations in Ta-10W

Stephen M. Foiles
Computational Materials and Data Science Department
Sandia National Laboratories
Albuquerque, nm 87185

Abstract

It is well know that the addition of substitutional elements changes the mechanical behavior of metals, a effect referred to solid solution hardening. For body-centered-cubic (BCC) metals, screw dislocation play a key role in the mechanical properties. Here the detailed modification of the Peierls barrier for screw dislocation motion in Ta with W substitutional atoms is computing using density functional theory (DFT). A reduced order model (ROM) of the influence of W substitution on the Peierls barrier is developed. The mean field change in the Peierls barrier for a Ta10W alloy is determined and shown to be larger than anticipated based on simple elasticity considerations. The ROM could be used in future calculations to determine the local variability of the Peierls barrier and the resultant influence on the motion of screw dislocation in this alloy.

Acknowledgment

This work benefitted from discussions with Corbett Battaile, Hojun Lim and John Emery. It was supported by the Advanced Simulation and Computing (ASC), Physics & Engineering Models program through the Predicting Performance Margins (PPM) program.

Contents

Appendix

List of Figures

List of Tables

Nomenclature

Ta Tantalum

W Tungsten

DFT Density Functional Theory based electron structure calculations

VASP Vienna Ab Initio Simulation Package

NEB Nudged Elastic Band

BCC Body Centered Cubic crystal structure

ROM Reduced Order Model

Chapter 1

Introduction

The deformation of metals is dominated by the motion of dislocaitons. For the case of body-centered-cubic (BCC) structured metals, the deformation is strongly influenced by the motion of $\frac{1}{2}\langle 111\rangle$ screw dislocaitons [2, 1] and the nature of the slip systems has been reviewed by Weinberger, et al [18]. The motion of the screw dislocations is thermally activated and rate dependent due to the Peierls barriers that the screw dislocations need to overcome and which results from the non-planar core of the screw dislocation [3]. These properties of the screw dislocation impart the characteristic temperature and strain rate dependent behavior of the flow stress. The incorporation of the temperature and straiin rate dependencies is critical to the development of crystal plasticity models of the deformation of BCC metals.

The structure of the screw dislocation core in various elemental BCC metals has been the subject of multiple studies over the years as reported in multiple reviews including a recent review by Vitek and Paidar [17]. In these studies the dislocation core is observed to spread into three $\{1\ 1\ 0\}$ planes for the $\frac{1}{2} < 111 >$ screw dislocaiton. Gröger and Vitek completed an extensive analysis of the motion of the screw dislocations based on a sophisticated interatomic potential model [3, 4, 5]. The Peierls barriers for various elemental BCC metals has recently been calculated by density functional theory (DFT) electronic structure calculations[19].

The focus of this study is the influence of alloying on the resultant mechanical properties, in particular the temperature and strain rate dependent flow stress of the alloying. The influence of solid solutions on the mechanical properties of metal and the motion of dislocation in particular has a long history as summarized by, for example, Haasen [6]. The classic theory of solid-solution hardening in a concentrated solid solution is credited to Mott and Labusch [12, 11]. This theory posits a distance dependent interaction between the substitutional atoms and the dislocation core and also an average distribution of substitutional atoms around the dislocation. These assumptions lead to an average interaction of the dislocations with the alloy additions.

One of the current focuses of materials research is the variability of materials properties. That has led to the question to be address here, what is the local variability of the interaction of the dislocation with the statistical distribution of impurities. To that end, this report presents the development of a reduced order model (ROM) that allows for the ready evaluation of the local Peierls barrier from a particular local arrangement of W atoms in the Ta10W alloy. Future work would determine the influence of this local variation on the mechanical properties.

In considering the interaction of dislocations with a solute field, there are two kinetic limits that one can consider, sessile and mobile dislocations. For sessile dislocations, one would expect the distribution of solutes to equilibrate to the strain field of the dislocation and create a Cottrell atmosphere [7]. For mobile dislocations, the solute distribution would not be in equilibrium with the dislocation position, but rather would be distributed statistically consistent with the inherent short-range ordering in the alloy. In this report, mobile dislocations are considered, though the extension to sessile dislocations is possible.

Chapter 2

Elasticity Predictions

Since the dominant aspects of dislocation structure and energetics are strongly influenced by elasticity considerations, the influence of alloying on the elastic constants has been computed. These calculations are based on the standard density functional theory (DFT) electronic structure approach. The speciffic implementation used here is described in Appendix A.

DFT calculaitons of elastic constants are reported in Table 2.1 for Ta, Ta_7W and a random $Ta_{48}W_6$ alloy. For pure Ta, the experimentally observed bulk modulus, B, and shear moduli, C_44 and C', are 196 GPa, 83 GPa and 53 GPa, respectively [7]. These values agree well with the computed values obtained here. Two alloy configurations with compositions close to Ta10%W are considered. These model systems were chosen for computational convenience. The Ta_7W structure is an ordered arrangement obtained by a 2x2x2 repeat of the primitive BCC unit cell with one of the sites in this eight atom cell replaced by W. The $Ta_{48}W_6$ structure is based on a 3x3x3 repeat of the cubic BCC cell with W located at 6 randomly selected sites in this 54 atom cell. The similar elastic constants obtained for these two alloy structures (same values within the uncertainty of the DFT calculations) indicate that the influence of the W additions on overall elastic constants is not strongly dependent on the precise locations of the W solutes. Overall, the influence of the W alloying on the elastic moduli is modest. The main effect is a reduction in the anisotropy of the shear elastic constants. This is not surprising since the shear elastic constants of W are nearly isotropic.

Table 2.1: Bulk moduli (B), and shear moduli (C_{44} and C' = $\frac{1}{2}$(C_{11}-C_{12})) and lattice constants calculated by DFT for pure Ta, ordered Ta_7W and a random $Ta_{48}W_6$ configuration.

	Ta	Ta_7W	$Ta_{48}W_6$
B	200 GPa	209 GPa	205 GPa
C_{44}	84 GPa	77 GPa	77 GPa
C'	55 GPa	60 GPa	61 GPa
a	0.332 nm	0.330 nm	0.330 nm

The elastic energy of a dislocation is dictated by the relevant shear modulus of the dislocation. For the case of a screw dislocation, the relevant moduli are in the coordinate system where the z'-direction aligns with the screw dislocation line, $< 111 >$ [7]. The relevant moduli in this frame, denoted by a prime, are C'_{44}, C'_{55} and C'_{45}, and are related to the elastic moduli in the standard cubic orientation by equations 2.1 and 2.2. The pre-

logarithmic energy factor is given by 2.3. It was noted by Weinberger, et al. [19] that for a set of elemental BCC metals the magnitude of the Peierls barrier for the motion of the screw dislocation scaled with the pre-logarithmic energy factor. The prelogarithmic energy factors are 4.25, 4.27 and 4.31 $10^{-10} J/m$ for Ta, Ta_7W and $Ta_{48}W_6$, respectively. These values agree within the typical errors associated with DFT predictions of lattice constants and elastic constants. Thus, *if this correlation persists for the case of alloys*, one expects only a modest change in the magnitude of the Peierls barrier for the alloy compared to pure Ta.

$$C'_{44} = C'_{55} = \frac{1}{3}(C_{11} - C_{12} + C_{44}) \tag{2.1}$$

$$C'_{45} = 0 \tag{2.2}$$

$$K = \frac{\sqrt{C'_{44}C'_{55} - {C'_{45}}^2}b^2}{4\pi} \tag{2.3}$$

Standard elasticity arguments also predict that the interaction of W substitutional atoms with screw dislocation will be small outside of the core. (The strain fields at the dislocation core are large, so it is unlikely that elasticity predictions will be realistic.) The first term in the elastic interaction is the interaction of the hydrostatic stress field with the misfitting sphere of the substitutional. For W in Ta, the change in lattice constants with alloying suggest that the volume misfit is -3 Å^3. In addition, for isotropic elasticity, there is no hydrostatic stress field around a screw dislocation. While Ta is anisotripic, the hydrostatic stress should be small. The next level of interaction is the modulus interaction [7] given by equation 2.4.

$$\Delta E = \frac{1}{2}\epsilon_{ij}\epsilon_{kl}\Omega\Delta c_{ijkl} \tag{2.4}$$

In this equation, ϵ is the strain tensor, Ω is the atomic volume and Δc is the local change in elastic constants. For the screw dislocation, the elastic constants that couple to the strain field are the ones given in equation 2.1 which do not change significantly with the addition of W. Thus, simple elasticity ideas suggest that the long-range interaction of W substitutions in Ta with the screw dislocations should be small.

Chapter 3

Development and Testing of Reduced Order Model

We will employ density functional theory (DFT) calculations to determine the interaction of W substitutional atoms with the screw dislocation in Ta and to determine the change in the local Peierls barrier due to the substitutional atoms. The DFT calculations employed use standard techniques as described in Appendix A. These DFT calculations require the use of periodic boundary conditions. It is topologically not possible to simulate a single dislocation with periodic boundary conditions in all three dimensions. The net Burgers vector content of each periodic unit cell must be zero. One option is to simulate a dislocation dipole as indicated schematically in Figure 3.1a. This geometry has been used in various computational studies. A potential issue with this geometry is that due to the periodic boundary conditions, one is actually simulating a set of repeating dislocations that form low-angle grain boundaries. Thus there is a repeating pattern of grain rotations due to the presence of the alternating low-angle grain boundaries. An alternative simulation geometry is to form a dislocation quadrapole as in shown schematically in Figure 3.1b. This arrangement avoids the creation of grain boundaries. The use of non-orthogonal periodic vectors also allows this geometry to be created with only two dislocations in the periodic cell.

The details of the construction of this primitive unit cell have been presented previously and so will not be repeated here [13, 19]. Initial DFT computational cell is shown in Fig. 3.2. In this figure the shading reflects the local crystal structure as determined using common neighbor analysis. The blue atoms are BCC while the white atoms are classified as other. In this case, the white atoms are located at the core of the screw dislocation. Note that as discussed in ref. [13] there is a uniform shift of half a Burgers vector of the atom positions in the direction normal to the figure as one moves from the lower right hand corner to the upper left corner. Further note that this basic unit cell has a periodic length of a Burgers vector, or equivalently a nearest neighbor distance, in the direction normal to the plane of the figure.

The calculaition of the Peierls barrier is performed using nudged elastic band (NEB) simulations[15, 8]. These simulations require the specification of an initial and final state. Here the final state has the dislocation core shifted to the left in Fig. 3.2 by one atomic site. A set of intermediate states of the system are then generated and the energy of these intermediate states are minimized while also minimizing the displacements between the im-

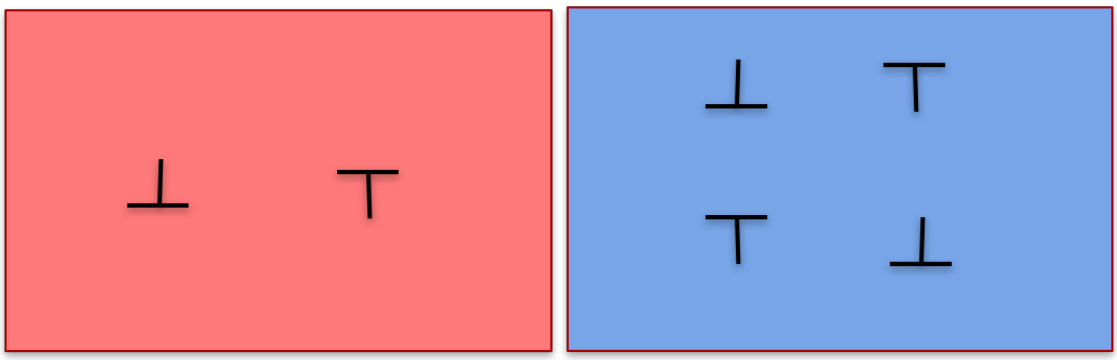

(a) dipole geometry (b) quadrapole geometry

Figure 3.1: Schematic illustration of the (a) dipole and (b) quadrapole arrangement of dislocations in the computational cell.

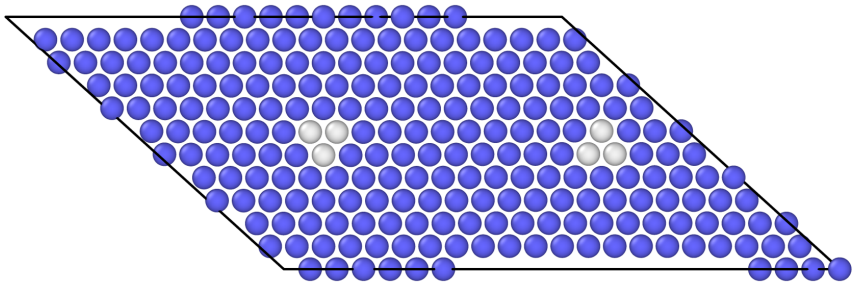

Figure 3.2: Atomic structure for the DFT calculations. Note that the cell is periodic and there is a overall displacement normal to the figure as discussed in the text. The shading is based on common neighbor analysis with the blue atoms being BCC environments and the white atoms being other.

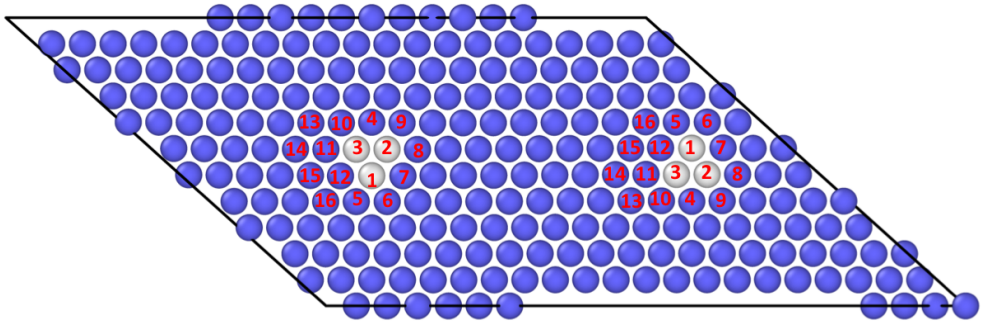

Figure 3.3: Atomic structure for the DFT calculations. The numbers identify the sites where W substitution will be considered with W substitutions being performed simultaneously at both dislocation cores. The shading is based on common neighbor analysis with the blue atoms being BCC environments and the white atoms being other.

ages. These calculations employ nine intermediate states. The barrier for the case of pure Ta is shown as the bottom curve in Fig. 3.4. This barrier is in good agreement with the one calculated earlier using the same techniques[19].

Fig. 3.3 shows the initial structure with the sites where W substitution will be considered idenitified by number. This numbering system will be used here to identify the different locations. Note that W substitutions are added symmetrically to the cores of both dislocations in the computational cell. These sites represent all the locations which are in the core triangle or the sites adjacent to the core triangle for either the initial or the final dislocation position. This is the reason for the inclusion of sites further to the left of the initial dislocation region.

The Peierls barrier for both pure Ta and with a W substitutional at 5 of the sites is shown in Fig. 3.4. The barrier for the other sites were also calculated but are not shown here for simplicity. Note that the calculations for some of the sites can be related to the barriers for other sites via symmetry arguments. For example, the reaction path for the barrier associated with W placement at site 12 is the just the reverse direction of the reaction path for the barrier calculation at site 1.

The data in Fig. 3.4 shows the interaction energy of the W substitutional with the dislocation core which is the value of the energy change for a reaction coordinate of 0. The reaction coordinate is a measure of the fraction of the distance from the initial state to the final state. This indicates that the W substitutional has a significant interaction with the screw dislocation core of about 0.22-0.23 eV. Due to the symmetric structure of the core, one would expect the impurity energy to be the same for sites 1, 2 and 3 for an infinite system. The difference between these values reflects the fact that the computational cell employed here does not have the same three-fold symmetry as the ideal dislocation core. Thus the computed energy for these three sites differs. This difference can have two sources. The first would be potential interactions, either electronic or elastic, between the W substitutional atoms in the array of cores. This array does not have the three-fold symmetry. The second possible origin is numerical differences in the DFT calculations due to the differences between

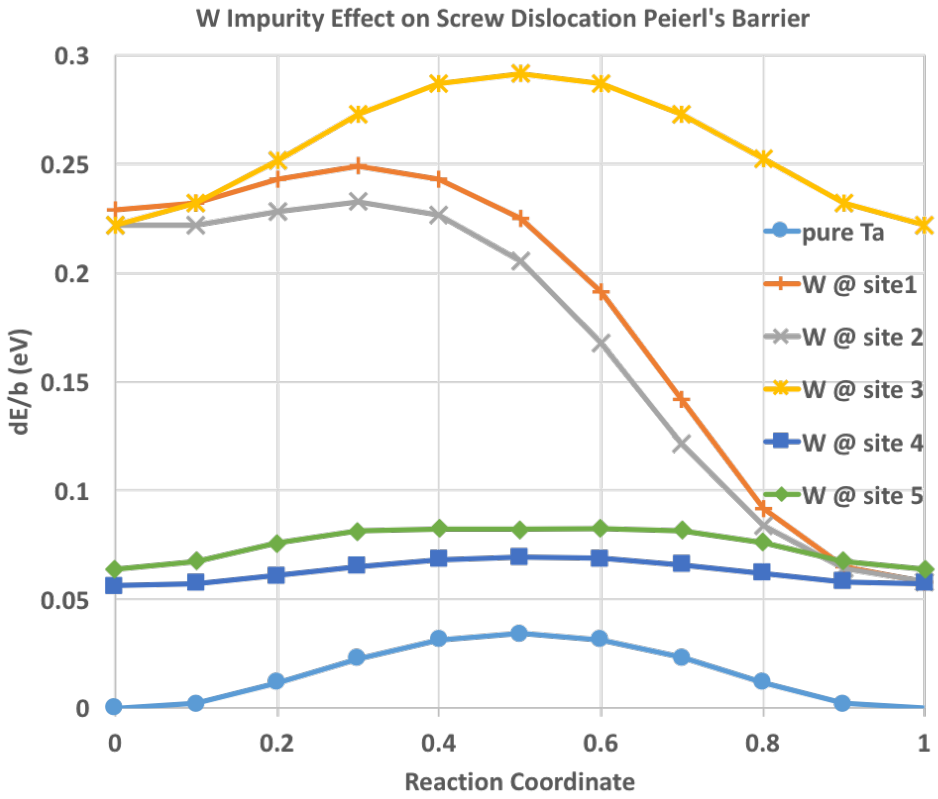

Figure 3.4: Peierls barrier computed using DFT energies and NEB method for both pure Ta and for systems with a W substitutional atom at 5 sites in or near the dislocation cores as defined in Fig. 3.3. The energy is in electron volts per Burgers vector of length. These energies represent a single impurity since the raw energy changes have been devided by two to reflect the symmetrical placement of W at the two dislocation cores in the computational cell.

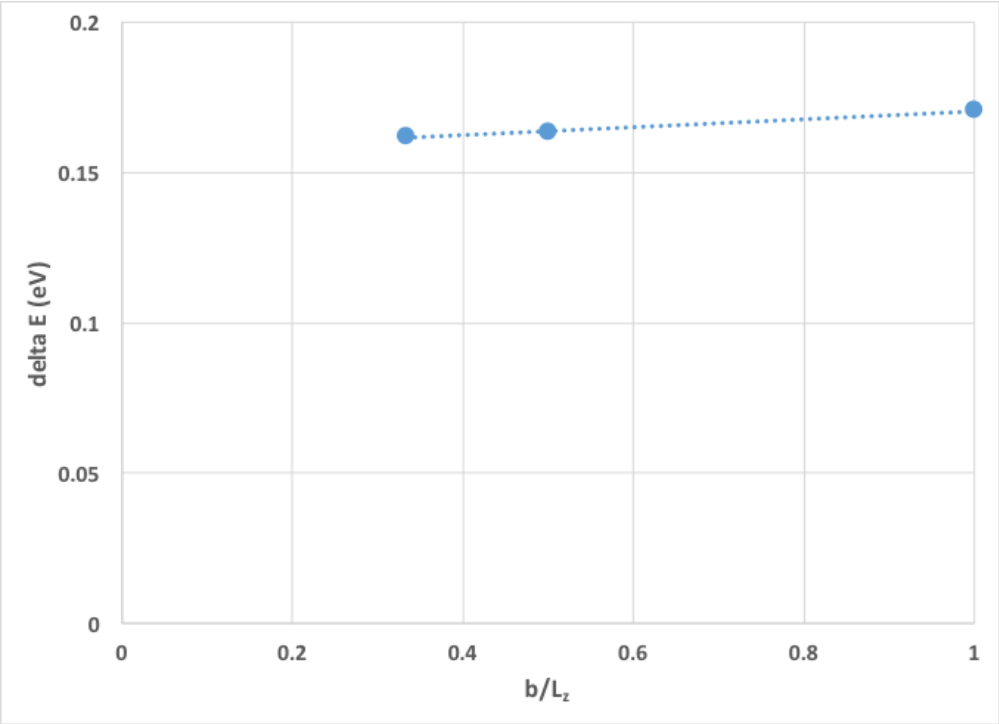

Figure 3.5: Energy change associated with adding a single W impurity at site 1 of each dislocation core as a function of the inverse length of the computational cell along the dislocation line.

the symmetry of the computational cell and that of the core. The observed difference is on the order of 0.01 eV. This gives a qualitative sense of the scale of the computational uncertainties. These differences are smaller than the effects of importance here. The interactions of the W substitutional atoms at sites 4 and 5 adjacent to the core is substantially reduced compared to the interaction with the core, but is still significant at about 0.06 eV. Similar results have been obtained for W substitutions in all of the 16 sites identified in Fig. 3.3.

The results presented in Figure 3.4 were obtained for a computational cell which is 1 Burgers vector or equivalently one nearest neighbor distance thick. This means that these calculations are actually for the dislocation interacting with a infinite column of W substitutional atoms located in nearest neighbor sites. This is not consistent with a dislocation moving through a statistical distribution of substitutional atoms. In particular, the short-range order in Ta-W disfavors W nearest neighbors. For this reason, it is crucial to establish the relationship between these calculations and isolated W substitutional atoms. To this end, the calculation of the energy of a W substitutional at site 1 was repeated for cells whose length along the dislocation line is two and three times the Burgers vector. For these calculation, there is still only W atom per dislocation core. The resulting change in energy for the system with the W substitutional compared to the system of the same size without the W is presented in Figure 3.5. The main result is that the interaction between the W substitutional and the dislocation core is weakly dependent on the separation of the W atoms along the dislocation core. The decrease in interaction energy as the separation between the

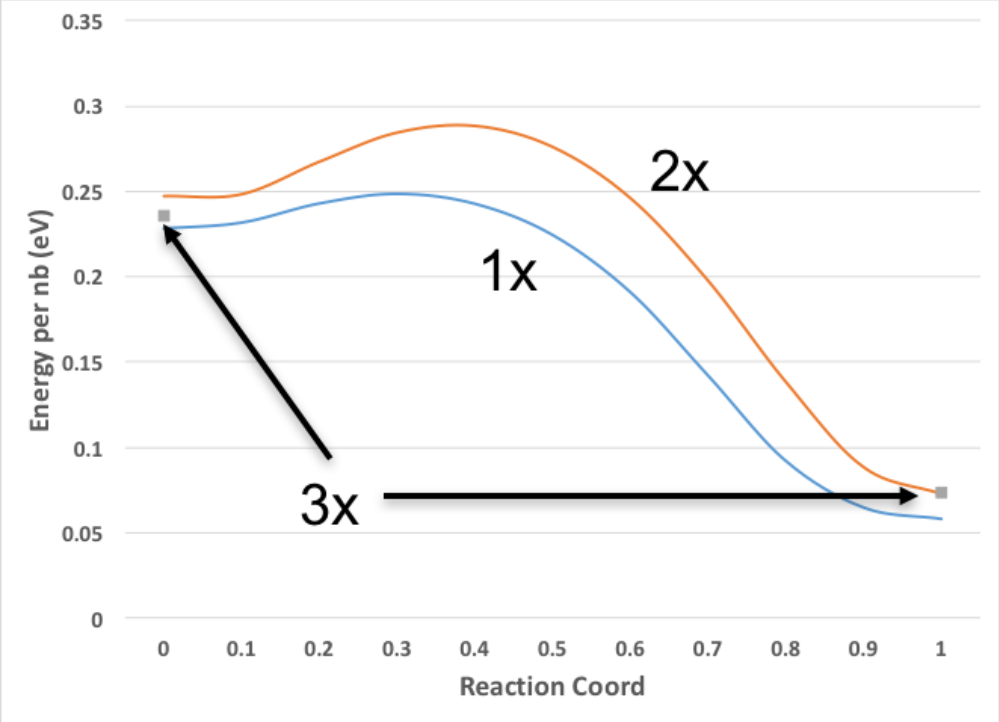

Figure 3.6: Peierls barrier for W substitutional at site 1 for different lengths along the dislocation line. Note that for 3x (length of 3 Burgers vectors along the dislocation line) only the endpoints are given.

W atoms increases is also consistent with the short-range order tendency of the alloy.

Figure 3.6 shows the calculation of the Peierls barrier for a computational cell that is 2 Burgers vector thick compared to the prior calculation of the barrier for a single layer thickness. Note that this is an energy per unit length. Qualitatively, the position of the maiximum in the barrier for the twice thickness calculation is closer to a reaction coordinate of 0.5 and the magnitude of the increase in the barrier from the starting point to the maximum is larger than for the case of the cell with a single layer thickness. This suggests that the barrier in the case of the 2 layer thickness is approximately the average of the barrier for the case of the 1 layer thickness and the barrier with no W substitutional.

This observation suggests a very simple reduced order model of the barrier. To compute the barrier for n-layer system with W substitutional atoms at locations j where the sum is over all locations j where there are W substitutional atoms. In this equation, the superscript n-layer refers to a cell which is n Burger vector thick and single superscript refers to the calculation for the cell that is a single Burgers vector thick. The subscript pure means the calculation for no substitutional atoms and the subscript j refers to a system with the W substitution at location j and the subscript {j} refers to the system with the substitutions at the set of sites {j}. The numerical data required for the implementation of Equation 3.1

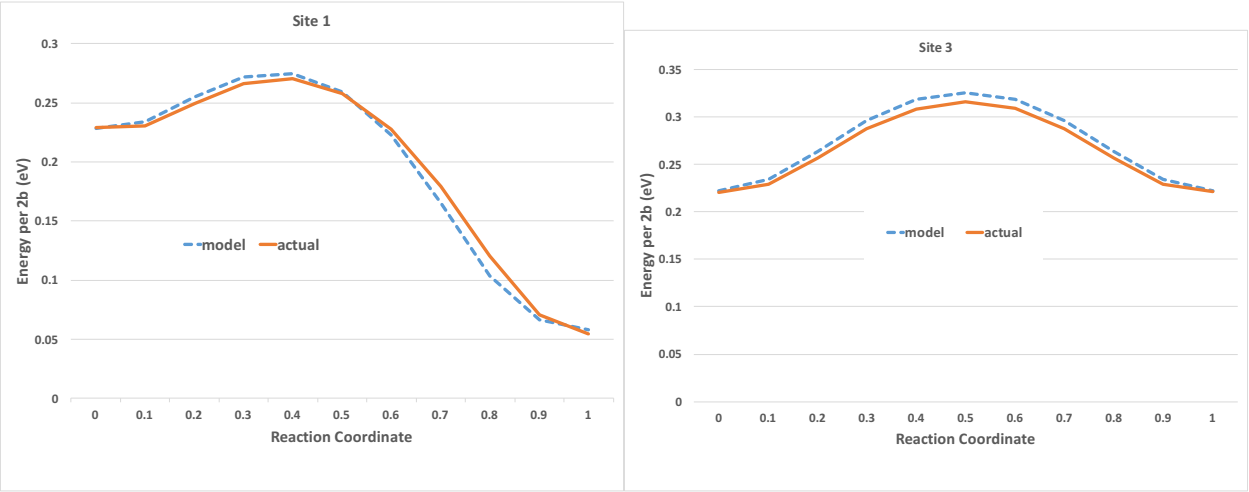

(a) site1 (b) site3

Figure 3.7: Comparison of the the computed Peierls barrier for a cell 2 Burgers vector long along the dislocation line compared to the prediction of the reduced order model (see text) for W substitutional at (1) site 1 and (b) site 3.

is presented in Appendix B.

$$dE_{\{j\}}^{n-layer}(x) = dE_{pure}^{n-layer}(x) + \sum_{j}[dE_{j}^{single}(x) - dE_{pure}^{single}(x)] \tag{3.1}$$

The applicability of Equation 3.1 is tested for two simple cases in Figure 3.7. The full calculation in Figure 3.7a shown by the solid line is the same as that in Figure 3.6. The dashed line shows the prediction of Equation 3.1. The results in Figure 3.7b are the same except for the placement of the W substitutional atom at site 3. In both cases, the agreement between the full calculation and the reduced order model (ROM) is quite good. A more demanding test of the ROM is summarized in Figure 3.8 and Figure 3.9. Two random placements of W substitutional atoms where generated at 10% concentration of W. In this generation, nearest neighbor W were avoided but otherwise the placement of the W atoms was at random. Both of the cell in Figure 3.8 are 2 layers thick and W atoms are placed in both layers. The Peierls barrier was then computed by a full DFT calculation for each of these configurations. These results in the solid lines are compared with the prediction of the ROM in dashed lines in Figure 3.9. Given the complexity of the arrangement, the agreement between the full calculation and the ROM are reasonably good. In particular, note that the ROM only considers the infuence of the W substitutional atoms in the immediate vicinity of the the initial or final location of the dislocation core, the 16 sites identified in Figure 3.3. The remaining substitutional atoms are not considered. While they are not expected to have a large effect, neglecting them is clearly a simplification. This establishes that the ROM can be reliably used to estimate the local Peierls barrier even for W concentrations as high as 10%.

In evaluating the accuracy of the ROM, it is important to keep the computational effi-

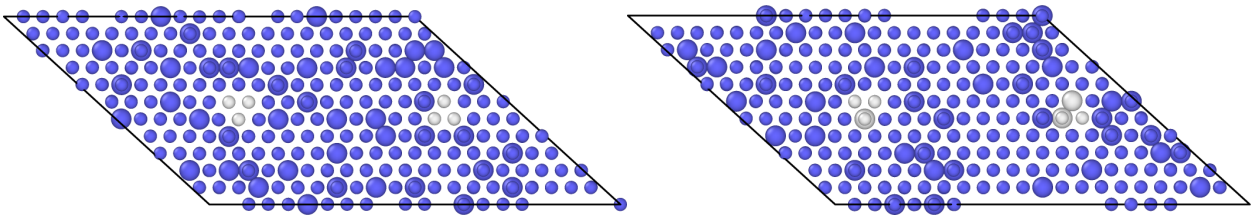

(a) (b)

Figure 3.8: Two structures with random substituion of W in the computational cell. The cell contains two periods along the dislocation line (normal to the plane of the figure). The shading is based on common neighbor analysis, the size reflects the species with W drawn larger.

ciency in mind. The brute force barrier calculations presented in Figure 3.9 each required substantial computing resources. These calculations used 128 cores for the DFT calculations associated with each of the 11 replicas in the NEB calculation for a total of 1,408 cores. These calculations ran for approximately three wall-clock days each. Thus each of these curves represents about 11.5 cpu-years of computing. While this is feasible for a small number of calculations on a large computer cluster, it is prohibitive to perform such brute-force calculations for a sufficiently large number of arrangement to obtain statistical averages. By comparison, the calculations required to calibrate the ROM required about a quarter of the computer resources of a 2-layer brute-force calculation. The computational effort for the evaluation of the barrier based on the ROM is negligible. This enables the statistical sampling of barriers that may be encountered as discussed in the next chapter.

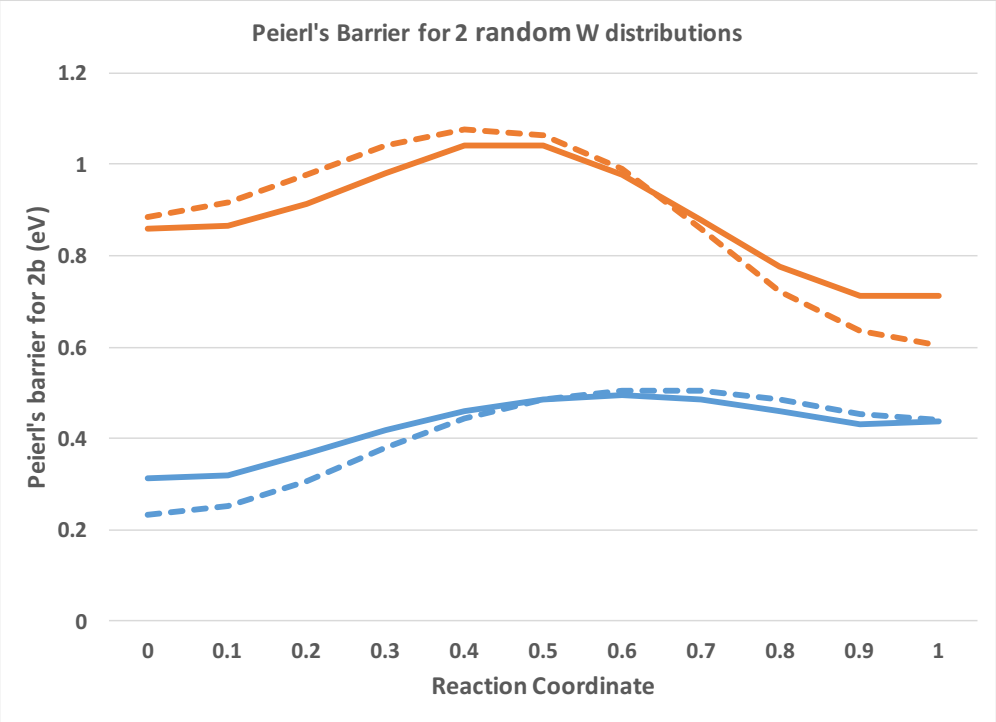

Figure 3.9: Peierls barrier calculation (solid line) for the two random arrangements of W substitutional atoms shown in Fig. 3.8 compared with the predictions of the ROM (dashed lines). The upper curves are for Fig. 3.8a and the lower curves are for Fig. 3.8b.

Chapter 4

Predictions of Reduced Order Model

The value of the ROM is that it can be used to predict the energy landscape for a variety of potentials local configurations of the substitutional atoms. This feature can either be used to quickly estimate the average influence of the substitutional atoms or it could be used to look at the range of local barriers that the dislocation might encounter.

The simplest statistical sampling for Ta-10W of the W distribution is a mean field model in which the each site in Equation 3.1 is assumed to be one tenth occupied by W. Physically, this can also be thought of as the energy per unit length of an infinite straight dislocation moving through a random distribution of W substitutionals. The mean field barrier is shown in Figure 4.1 compared to the Peierls barrier for pure Ta. Note that the mean field barrier is predicted to be approximately 40% higher in Ta-10W than in pure Ta. Recall that the correlation between Peierls barrier and the pre-logarithmic energy factor observed by Weinberger, et al. [19] for elemental materials predicted that the Peierls barrier would be largely unchanged based on the variation of the elastic constants. This indicates that this simple correlation between Peierls barriers and elastic constants does not extend to the additional local behavior that is obtained for alloy systems.

Figure 4.2 presents two illustrations related to the local variation of the Peierls barrier. The mean field barrier in Figure 4.1 can be intuitively thought of as the barrier per unit length of encountered by a perfectly rigid straight dislocation. Figure 4.2a presents the range of local barriers that would be encountered in the opposite limit where one computes the local barrier for each Burger's vector length segment of the dislocation. This limit is unphysical since it completely ignores the dislocation line energy which tends to straighten the dislocation in order to minimize the line energy. It does give a sense, though, of the local variations in the energy landscape. As can be seen, the local variations are much larger than the average barrier. A more realistic view of the local variation of the Peierl's barrier is shown in Figure 4.2b where the local barrier is averaged over 5 Burger's vectors lengths for a random distribution of substitutional atoms. This shows the reduction in the variability due to the local straightening of the dislocation due to the dislocation line length. The variation is substantially reduced compared to Figure 4.2a but is still on the order of the average barrier. These results suggest that the inclusion of the local barrier variability may have a significant influence on the dynamics of the screw dislocation motion.

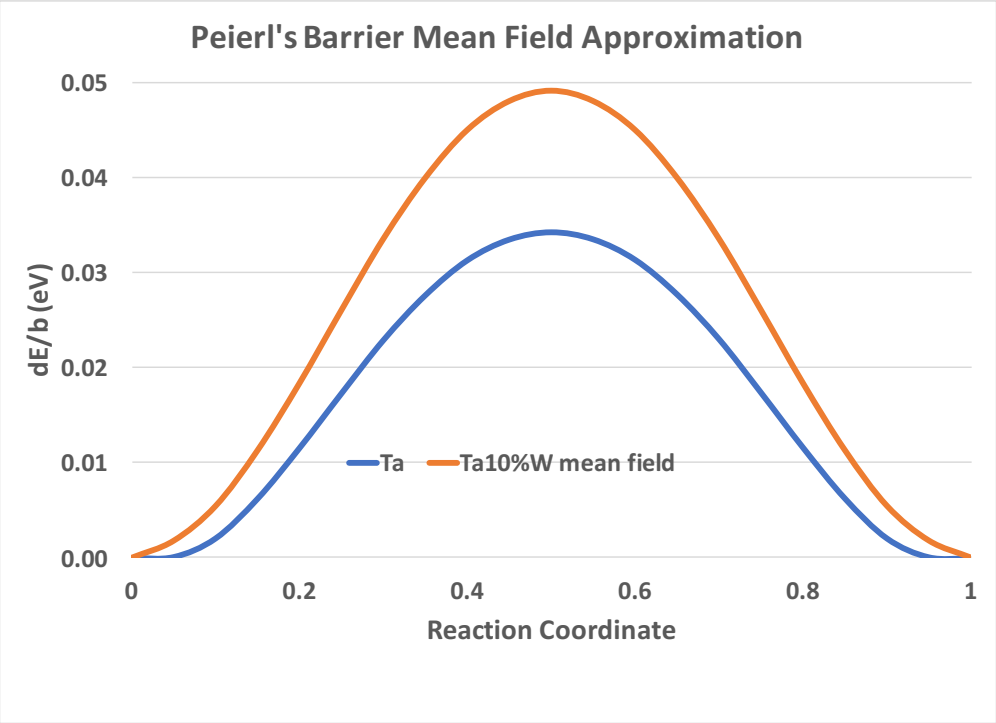

Figure 4.1: Peierls barriers computed for pure Ta [19] and obtained for Ta10W based on the reduced order model and a mean field treatment of the W locations.

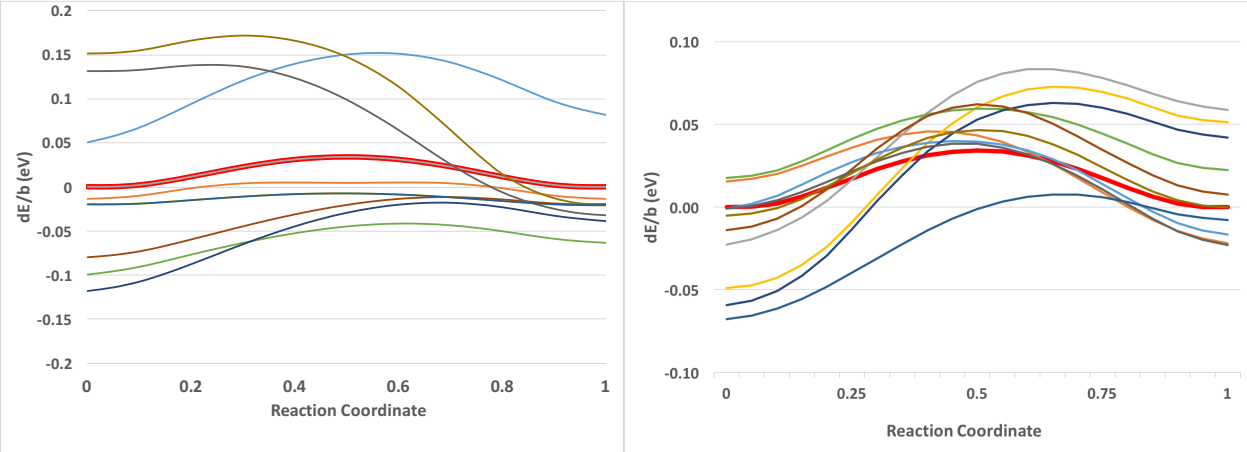

(a) (b)

Figure 4.2: Local Peierls barrier obtained for various random distributions of W averaged over (a) a single Burgers vector along the dislocation line and (b) five Burgers vector along the dislocation line. The thick red line is the Peierls barrier for pure Ta.

Chapter 5

Future Directions

The present work reveals that the local energy landscape through which a dislocation in Ta-10W moves is far from smooth. This raises questions about whether the motion of the screw dislocation will behave in a manner that is qualitatively different from that in pure Ta. For the pure BCC metals, there are two regimes of dislocation motion depending on both the temperature and strain rate, the kink-pair regime and line tension regime [14]. Each of these regimes has a distinct temperature dependence of the thermal part of the flow stress.

The logical next step for this work is to develop a simple model for the motion and equilibrium configurations for a screw dislocation in a statistical distribution of W substitutional atoms. This model would incorporate local barriers along the dislocation line based on the ROM developed in this report. This energy would be supplemented by the line energy of the dislocation which as discussed above would tend to locally straighten the dislocation. Such a model could then be employed to determine of the response of screw dislocation to an applied stress is more in line with the kink-pair picture, the line tension picture or possible a different mesoscale description. Such insight would facilitate the development of temperature, strain-rate and pressure dependent crystal plasticity models such as has been done for elemental Ta [14].

References

[1] A. Argon. *Strengthening Mechanisms in Crystal Plasticity*. Oxford University Press, 2008.

[2] D. Caillard and J. L. Martin. *Thermally Activated Mechanisms in Crystal Plasticity*. Pergamon, 2003.

[3] R. Gröger, A. G. Bailey, and V. Vitek. Multiscale moldeling of plastic deformation of molybdenum and tungsten: I. Atomistic studies of the core structure and glide of $1/2\langle 111\rangle$ screw dislocations at 0 K. *Acta Materialia*, 56:5401–5411, 2008.

[4] R. Gröger, V. Racheria, J. L. Bassani, and V. Vitek. Multiscale modeling of plastic deformation of molybdenum and tungsten: II. Yield criterion for single crystals based on atomistic studies of glide of $1/2\langle 111\rangle$ screw dislocations. *Acta Materialia*, 56:5412–5425, 2008.

[5] R. Gröger and V. Vitek. Multiscale modeling of plastic deformation of molybdenum and tungsten iii. effects of temperature and plastic strain. *Acta Materialia*, 56:5426–5439, 2008.

[6] P. Haasen. Mechanical properties of solid solutions. In R. W. Cahn and P. Haasen, editors, *Physical Metallurgy*, volume 3, chapter 23, pages 2010–2073. North-Holland, fourth, revised and enhanced edition edition, 1996.

[7] J. P. Hirth and J. Lothe. *Theory of Dislocations*. Wiley-Interscience, second edition edition, 1982.

[8] H. Jonsson, G. Mills, and K. W. Jacobsen. Nudged elastic band method for finding minimum energy paths of transitions. In B. J. Berne, G Ciccotti, and D. F. Coker, editors, *Classical and Quantum Dynamics in Condensed Phase Simulations*. World Scientific, 1998.

[9] G. Kresse and J. Furthmuller. Efficient interative scheme for ab initio total-energy calculations using a plane-wave basis set. *Physical Review B*, 54(16):11169–11186, 1996.

[10] G. Kresse and D. Joubert. From ultrasoft pseudopotentials to the projector augmented-wave method. *Physical Review B*, 59:1758–1775, 1999.

[11] R. Labusch. Statistical theories of solid-solution hardeing. *Acta Metallurgica*, 20:917, 1970.

[12] R. Labusch. A statistical theory of solid solution hardening. *Physical Status Solidi*, 41:659, 1970.

[13] J. Li, C.-Z. Wang, J.-P. Chang, W Cai, V. V. Bulatov, K.-M. Ho, and S Yip. Core energy and peierls stress of a screw dislocation in bcc molybdenum: A periodic-cell tight-binding study. *Physical Review B*, 70:104113, 2004.

[14] Hojun Lim, C. C. Battaile, J. L. Brown, and C. R. Weinberber. Physically-based strength model of tantalum incorporating effects of temperature, strain rate and pressure. *Modelling and Simulation in Materials Science and Engineering*, 24:055018, 2016.

[15] G. Mills, H. Jansson, and G. K. Schenter. Reversible work transition state theory: application to dissociative adsorption of hydrogen. *Surface Science*, 324:305, 1995.

[16] H. J. Monkhurst and J. D. Pack. Special points for brillouin-zone integrations. *Physical Review B*, 13(12):5188–5192, 1976.

[17] V. Vitek and V. Paidar. Non-planar dislocation cores: A ubiquitous phenomenon affecting mechanical properties of crystalline materials. In J. P. Hirth, editor, *Dislocations in Solids*, volume 14, chapter 7. Oxford, 2008.

[18] C. R. Weinberber, B. L. Boyce, and C. C. Battaile. Slip planes in bcc transition metals. *International Materials Reviews*, 58(5):296–314, 2013.

[19] C. R. Weinberger, G. J. Tucker, and Foiles S. M. Peierls potential of screw dislocations in bcc transition metals: Predictions from density functional theory. *Physical Review B*, 87:054114, 2013.

Appendix A

DFT Calculations

The electronic structure calculations are performed using the Vienna Ab Initio Simulation Package (VASP) [9]. This is a widely-used plane-wave basis set implementation of density functional theory (DFT) approximation to quantum mechanics. These calculations employed the generalized gradient approximation (GGA) with psuedopotentials of the projector-augmented-wave form (PAW) [10]. The pseudopotentials are taken from the VASP library version 5.2. The numbers of valence electrons treated are 11 and 12 for Ta and W respectively. The calculations were non-spin-polarized so assumed a paramagnetic state. For calculations involving multiple elements, it is important to use the same energy cut-off for the plane-wave basis. The energy cut-off employed in these calculations is 280 eV which is greater than the recommended high prescision cut-off for both elements. The k-space integrations are performed using the automatic mesh generation. The length (see VASP documentation) employed to generate this mesh was 40Å which was determined by convergence tests on a single W impurity in bulk Ta. For the dislocation cell with a single Burgers vector along the z-axis this led to a mesh with 16 irreducible points. The nudged elastic band (NEB) calculations[15, 8] were performed using the algorithm implemented in the VASP code with 9 intermediate configurations and the default spring setting.

Appendix B

Barrier Data

Table B.1 presents the computed values of the Peierls barrier for both pure Ta and Ta with a single W impurity located at each of the 16 sites identified in Figure 3.3. The reaction coordinate are listed in scaled units where 0 and 1 correspond to the initial and final configuration. The energies represent total computational cell energies in electron volts (eV). As discussed in the text, this data can be used in conjunction with Equation 3.1 to estimate the Peierls barrier for an arbitrary arrangement of W substitutional atoms.

reaction coord	pure	site 1	site 2	site 3	site 4
0	-2723.0359	-2725.2044	-2725.2176	-2725.2175	-2725.549
0.1	-2723.0318	-2725.1974	-2725.2181	-2725.1982	-2725.5469
0.2	-2723.0128	-2725.1749	-2725.2056	-2725.1576	-2725.5396
0.3	-2722.9901	-2725.1636	-2725.1965	-2725.1158	-2725.5314
0.4	-2722.9733	-2725.1753	-2725.2078	-2725.0881	-2725.5253
0.5	-2722.9674	-2725.212	-2725.2502	-2725.0787	-2725.5229
0.6	-2722.9732	-2725.2793	-2725.3257	-2725.0879	-2725.5245
0.7	-2722.9899	-2725.3774	-2725.4184	-2725.1154	-2725.5299
0.8	-2723.0127	-2725.4777	-2725.4938	-2725.1572	-2725.5378
0.9	-2723.0318	-2725.5324	-2725.5335	-2725.198	-2725.5454
1	-2723.036	-2725.5458	-2725.5452	-2725.2177	-2725.547

site 5	site 6	site 7	site 8	site 9	site 10
-2725.534	-2725.5367	-2725.5468	-2725.5454	-2725.5471	-2725.547
-2725.5268	-2725.5365	-2725.5444	-2725.5371	-2725.5388	-2725.5454
-2725.5098	-2725.529	-2725.5352	-2725.5183	-2725.5192	-2725.5378
-2725.4988	-2725.5234	-2725.5299	-2725.5048	-2725.4997	-2725.5299
-2725.4969	-2725.5253	-2725.534	-2725.504	-2725.4883	-2725.5245
-2725.4978	-2725.5373	-2725.5478	-2725.5164	-2725.4886	-2725.5229
-2725.4968	-2725.559	-2725.5694	-2725.5402	-2725.5016	-2725.5253
-2725.4986	-2725.5887	-2725.5967	-2725.5731	-2725.5262	-2725.5314
-2725.5097	-2725.6217	-2725.6266	-2725.6103	-2725.5572	-2725.5396
-2725.5267	-2725.6506	-2725.6539	-2725.6422	-2725.5843	-2725.5469
-2725.534	-2725.6644	-2725.6673	-2725.6563	-2725.5954	-2725.549

site 11	site 12	site 13	site 14	site 15	site 16
-2725.5452	-2725.5458	-2725.5954	-2725.6563	-2725.6673	-2725.6644
-2725.5335	-2725.5324	-2725.5843	-2725.6422	-2725.6539	-2725.6506
-2725.4938	-2725.4777	-2725.5572	-2725.6103	-2725.6266	-2725.6217
-2725.4184	-2725.3774	-2725.5262	-2725.5731	-2725.5967	-2725.5887
-2725.3257	-2725.2793	-2725.5016	-2725.5402	-2725.5694	-2725.559
-2725.2502	-2725.212	-2725.4886	-2725.5164	-2725.5478	-2725.5373
-2725.2078	-2725.1753	-2725.4883	-2725.504	-2725.534	-2725.5253
-2725.1965	-2725.1636	-2725.4997	-2725.5048	-2725.5299	-2725.5234
-2725.2056	-2725.1749	-2725.5192	-2725.5183	-2725.5352	-2725.529
-2725.2181	-2725.1974	-2725.5388	-2725.5371	-2725.5444	-2725.5365
-2725.2176	-2725.2044	-2725.5471	-2725.5454	-2725.5468	-2725.5367

Table B.1: Tabulation of the barriers as a function of the reaction coordinate for a single W impurity at the indicated site. The energy values are in units of electron volts (eV).

DISTRIBUTION:

	MS	,
		,
1	MS 0899	Technical Library, 9536 (electronic copy)


Sandia National Laboratories